MIT Open Access Articles

Dysregulation of dopamine receptor D2 as a sensitive measure for Huntington disease pathology in model mice

Massachusetts Institute of Technology

Dysregulation of dopamine receptor D2 as a sensitive measure for Huntington disease pathology in model mice

Zachary R. Crook and David E. Housman[1]

Koch Institute for Integrative Cancer Research, Massachusetts Institute of Technology, Cambridge, MA 02139

The ability to quantitatively evaluate the impact of a potential therapeutic intervention for Huntington disease (HD) in animal models for the disease is a critical step in the pathway to development of an effective therapy for this devastating neurodegenerative disorder. We report here an approach that combines a cell-based assay's quantitative accuracy and direct relationship to molecular processes with the ability to directly monitor effects in HD model mouse neurons. To accomplish this goal, we have developed an accurate quantitative reporter assay for a transcript known to be down-regulated as an early consequence of mutant *huntingtin* expression. This system uses mouse strains carrying a GFP reporter for the expression of the dopamine receptor D2, expressed in the medium spiny neurons of the basal ganglion. This receptor consistently demonstrates reduced expression in patients and murine models, and the FACS-based assay gives a highly accurate and quantitative readout of this pathology in mouse neurons expressing mutant *huntingtin*. For four genetic models and one viral model, a highly reproducible time course of loss of reporter expression is observed. This quantitative measure of HD pathology can be used to measure the effects of HD therapeutics in small cohorts with high confidence. We further demonstrate that the introduction of an shRNA against the *huntingtin* transgene by virus can improve this pathological status in medium spiny neurons transduced with the construct. We believe this system can be of great utility in the validation of effective therapeutic interventions for HD.

neurodegeneration | polyglutamine | viral vectors | gene expression | neuroprotection

In the search for effective therapeutic interventions for neurodegenerative diseases such as ALS, Parkinson disease, Alzheimer's disease, and Huntington disease (HD), cell and animal models for all of these conditions have been developed. Whereas cell models allow higher throughput and lower cost, any therapeutic intervention initially evaluated in a cell-culture model must subsequently be assessed in an appropriate animal model system before clinical trials in humans can be considered. However, the inherent variance in quantitation of the behavioral or pathological readouts in animals has practical consequences, requiring large cohorts to detect all but the most overt benefits, which limits experimental throughput. We sought to develop and implement an approach to this problem that combines the quantitative accuracy and direct relationship to molecular processes of a cell-based assay with the medical relevance of evaluating endogenous neurons in the animal brain.

In the present study, we have focused on HD. The uniform genetic etiology of HD, caused by a poly(CAG) expansion within exon 1 of huntingtin (*HTT*) (1), has provided an excellent starting point for the derivation of animal models for the disease. A number of similar animal models have been developed and characterized by behavioral and/or morphometric assessments of pathology (reviewed in ref. 2).

To develop a quantitative, cell-based preclinical assay system for HD, we have focused on a well-characterized early feature of disease pathology in both these animal models and HD patients,

transcriptional dysregulation in the medium spiny neurons (MSNs) of the basal ganglion, a phenotype with substantial consistency among mouse models and between the models and patients (3–6). One such dysregulated gene, dopamine receptor D2 (*DRD2* or D2), shows high expression levels in MSNs of the indirect pathway (striatopalladial) of the basal ganglion, which are among the earliest to die in HD (reviewed in ref. 7). Measuring the binding of the D2 ligand raclopride using PET scanning demonstrates reduced levels of DRD2 in the basal ganglia at, or even before, the onset of overt disease (8, 9). Many mouse models for HD show a corresponding loss of *Drd2* expression early in the progression of neuronal pathology (3, 10, 11). Because mouse models of HD do not lose neurons in great numbers until very late in disease progression (12, 13), this reduction is likely on a cell-by-cell level.

Dopamine signaling, and hence dopamine receptor alterations, likely plays a significant role in HD pathology. Selected evidence includes studies demonstrating that knocking out dopamine transporter 1 in an HD mouse model accelerates aggregate formation (14), that dopaminergic input depletion by 6-hydroxydopamine treatment reduces striatal glutamate levels (15), and the fact that the only current FDA-approved drug for symptom management in HD is a VMAT2 inhibitor, tetrabenazine. Down-regulation of such receptors may be an indirect by-product of pathological transcriptional dysregulation, or a specific compensatory response by MSNs undergoing polyglutamine-induced stress.

The National Institutes of Health (NIH)-supported Gene Expression Nervous System Atlas (GENSAT) Project proved to be an excellent resource to identify a mouse *Drd2* reporter strain (16). Using BAC transgenic methodologies, this project has created many GFP reporter mouse lines, among which is a *Drd2*-GFP (D2GFP) reporter strain that appeared extremely well suited to our goals. Extensive characterization of this mouse strain by the GENSAT Project and others (17) demonstrates a clear correspondence to the expression pattern of the endogenous mouse *Drd2* gene.

HD mouse models carrying the D2GFP reporter transgene were constructed by crossing, and a rapid and reliable flow cytometry-based protocol for quantitatively assessing the GFP levels of MSNs in these animals was developed. We found that HD mouse models show highly reproducible reductions in GFP levels in indirect MSNs during the early stages of disease progression, and that per-cell levels of GFP eventually stabilize at reduced levels, even while other pathologic measures are known to continue progressing. Time courses for decline in transcription levels of the reporter for a series of mouse models expressing either full-length or N-terminal fragments of mutant huntingtin were evaluated, and viral vectors were used to both induce and

NEUROSCIENCE

ameliorate this phenotype. It is our hope that the availability of an effective, quantitative reporter system in the mouse brain for therapeutic intervention efficacy in HD will improve the rapidity with which therapeutic interventions for HD can be discovered, validated, and made ready for human clinical use.

Results

Improved Yield for Isolation of MSNs from Adult Mouse Striata. To robustly quantify the progression of transcriptional dysregulation in mutant HTT (mHTT)-expressing neurons, we optimized a previously reported protocol (18) for dissociation of D2GFP MSNs that originally gave limited yields (~1,200 GFP$^+$ cells per striatum) that were inadequate for our needs. The modified protocol increased the yield to 15,000–25,000 GFP$^+$ cells per adult striatum, a sufficient number. The throughput of this protocol is sufficiently high that one individual can prepare a dozen samples for flow cytometry in roughly 3 h.

Suspensions of MSNs were subjected to flow cytometry. Event-by-event raw GFP quantities were acquired and further processed to assign a GFP level to the population (and therefore the mouse). For confirmation that GFP$^+$, DAPI$^-$ events (Fig. S1 *A–H*) were indeed MSNs of the indirect pathway, these events from D2GFP mice were collected and transcript levels were compared with whole striata (Fig. S1*I*, black versus striped bars). The sorted events demonstrated significant enrichment of transcripts known to be characteristic of MSNs of the indirect pathway (*Drd2*, *Adora2a*, and *Penk*) as well as significant reduction of transcripts known to be enriched in direct-pathway MSNs (*Drd1a* and *Tac1*) (19, 20). The previously reported down-regulation (3, 11) of *Drd2*, *Adora2a*, and *Penk* in HD models was reproduced in the aged HD model R6/1 striatum (Fig. S1*I*, black versus gray bars), confirming that the D2GFP background does not significantly alter this phenotype.

Quantitation of GFP Levels in D2GFP MSNs by Flow Cytometry. Robust and consistent quantitation of GFP levels in MSNs required removal of contaminating subpopulations from analysis. Fig. 1 represents an example of the quantitation pipeline for a mouse of strain R6/1 at 16 wk of age. Initial backgating computationally filtered out events with forward and side scatter profiles inconsistent with that of GFP$^+$, DAPI$^-$ events (which contain intact Drd2$^+$ MSNs). In this example, the GFP values of GFP$^+$, DAPI$^-$ events from a control littermate (Fig. 1*A*, blue gate) and an R6/1 mouse (Fig. 1*B*, red gate) were exported. Overlaying them (Fig. 1*C*) allows one to qualitatively distinguish wild-type from HD model samples, but also demonstrates that each contains two subpopulations. This phenomenon was particularly apparent in older R6/1 and R6/2 mice, for which specifically gating the entire GFP$^+$ population was not possible without including a portion of the neighboring debris field. These subpopulations can be separated using expectation maximization and Gaussian means regression into two population distributions (Fig. 1*D*). It was determined that the high-GFP population demonstrated the lowest variance within cohorts, so for robust quantitation the mean of the high-GFP distribution is used as the GFP value of each mouse (Fig. 1*E*). Normalizing this R6/1 mouse to the control littermate revealed a reduction to 34.4% of control GFP. The minimal variance of this analysis is demonstrated in Fig. 1*F* for the entire 16-wk-old R6/1 cohort (six R6/1 and three control mice were overlayed, producing values of 34.5 ± 1.8% for R6/1 normalized to 100 ± 2.3% in controls).

We normalized each mutant mouse's GFP value to that seen in age-matched control animals processed simultaneously (when more than one control animal was processed on a given day, the average was used). Normalized data of many mutant mice of the same or similar age, processed on the same or different days, were aggregated for study in time courses.

D2GFP Loss Is Progressive in both Fragment and Full-Length HD Mouse Models. *R6/2 mice.* We systematically crossed D2GFP mice to a number of HD model strains and analyzed the time course of
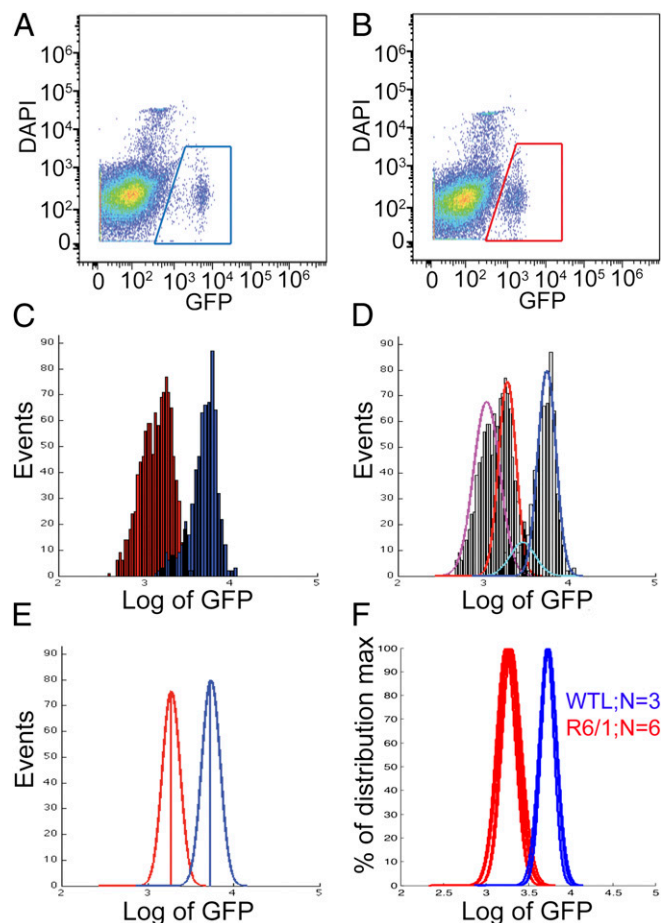

Fig. 1. Loss of D2GFP levels in HD model MSNs is visible by flow cytometry and can be robustly quantified. The GFP levels of GFP$^+$, DAPI$^-$ events (gated) from a wild-type littermate (*A*) and an HD model mouse (*B*; a 16-wk-old R6/1) in the D2GFP background were compared. The raw GFP values of these events (*C*) were processed by expectation maximization and Gaussian means regression scripts to assign two population distributions to the data (*D*). The mean of the high-GFP population (*E*) serves as an animal's GFP level. The minimal mouse-to-mouse variance of the assay can be readily visualized by overlaying all mice from a cohort on the same graph (*F*); this cohort contains six R6/1 and three WTL (wild-type littermate) mice. Red/pink are GFP$^+$, DAPI$^-$ events or distributions from R6/1 striata, and blue/cyan are those from WTL striata.

decline in GFP expression (Fig. 2*A*). Strain R6/2 is the product of strong expression of a transgene containing human *mHTT* exon 1 and its promoter (21). It has been widely used in the assessment of potential therapeutic interventions for HD (22, 23). We found that D2GFP expression in the MSNs of R6/2 showed significant differences from the values for wild-type littermates at the earliest age we evaluated, 4.5–5 wk of age. At this point, R6/2 GFP values were 80% of controls. As R6/2 animals aged, the differences in GFP values between R6/2 and control animals increased. Between 8 and 12 wk, when R6/2 animals decline precipitously in performance on behavioral tests (24), there was minimal further decline in normalized GFP levels between R6/2 and control, which remained in the range of 30–40%. The low variance of the measurements was demonstrated by power analysis (Table 1; power = 80%, alpha = 0.05), demonstrating that end-stage R6/2 mice (age 10.5–12 wk) would require only five animals to detect a modest 10% rescue of GFP levels.

R6/1 mice. A sister strain to R6/2 that has a similar transgene but delayed pathology, R6/1 mice (21), was also bred and tested at numerous time points. A similar progression to that seen in R6/2 was observed for R6/1 (Fig. 2*A*), with the expected delay of
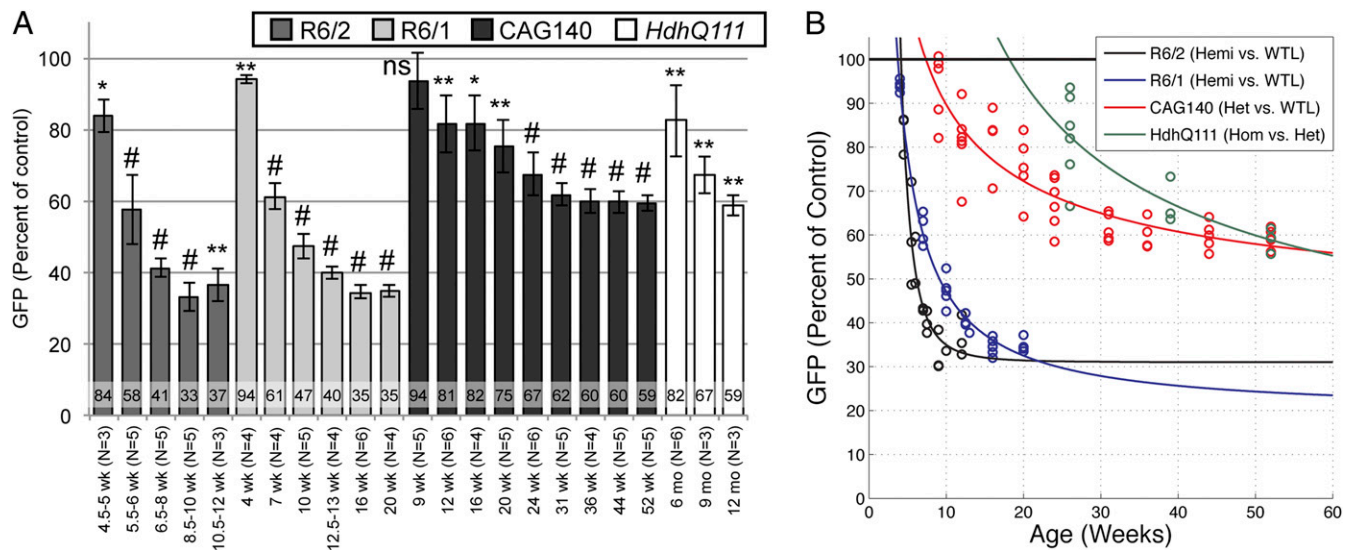
Fig. 2. HD model mice demonstrate a significant decline in D2GFP levels upon aging. Offspring of D2GFP mice and (from left to right) R6/2, R6/1, CAG140, and HdhQ111 strains were aged and MSNs were processed for quantification of GFP levels by flow cytometry. For R6/2, R6/1, and CAG140, hemi/heterozygotes were compared with wild-type littermates in analysis, with wild-type values set at 100. For HdhQ111 mice, homozygous mutants were compared with heterozygotes, also set at 100. Data are plotted in *A* organized by cohort, and in *B* as a scatter plot of GFP versus age. Error bars in *A* are SDs, and *P* values are from one-sample, two-tailed Student's *t* test versus a value of 100. ns, not significant. *$P < 0.05$, **$P < 0.01$, #$P < 0.001$. N for each cohort (hemi/heterozygotes for R6/2, R6/1, and CAG140; homozygotes for HdhQ111) is listed with the cohort's age. Using a power curve-fitting model (lines in *B*), analysis of the aggregated D2GFP loss among the HD model mice can be used to estimate both the age of onset (x value when y = 100) and the initial rates of decline of D2GFP (slope of the curve at y = 100) in the models.

progression. A subtle but statistically significant decline (to 94% of wild-type levels) was observed at 4 wk of age. GFP levels had declined precipitously by 7 wk of age in R6/1, plateauing at 35% of wild-type levels by 16 wk of age; no further decline was seen in 20-wk-old animals, when morbidity precludes further aging. Variance was even smaller in R6/1 mice than that seen in R6/2, possibly due to the uniform C57BL/6 background of R6/1. Power analysis in this strain (Table 1) suggests that detection of a 10% rescue in 7-wk-old mice requires only seven animals, and that by 16 wk of age, when D2GFP loss is no longer progressive, only three mice could reliably detect a 5% rescue. As estimated by power model curve fitting (Fig. 2*B*), R6/1 mice lose D2GFP at half the rate of R6/2 mice upon onset (23%/wk in R6/1 vs. 54%/wk in R6/2), although the age of onset is ~4 wk for both strains.

CAG140 mice. Knockin models of HD either introduce an expanded CAG repeat into exon 1 of mouse *Htt* or have the *Htt* gene modified to contain a hybrid human/mouse exon 1 with an expanded CAG repeat. In contrast to the R6 lines, most knockin lines (including CAG140 and HdhQ111) show no reduction in lifespan (25, 26), even when bred to homozygosity. However, heterozygous CAG140 mice (Fig. 2*A*) demonstrated significant GFP loss as early as 12 wk of age, to 81% of controls. D2GFP decline progresses through 31 wk of age before plateauing at ~62% of wild type. This D2GFP loss is before the reported rotarod latency deficit, and is also before the age at which reliable detection of *Drd2* loss by in situ hybridization is reported (27). Before plateauing, this strain demonstrates greater variance at the younger ages tested. Normalized GFP values ranged between 92% and 68% of wild-type values at 12 wk of age and between 74% and 59% of wild-type levels at 24 wk of age. However, by 31 wk of age, when progression had halted, variance was small enough that power analysis (Table 1) suggests only six mice would be sufficient for detection of a 10% rescue in GFP loss. Curve fitting (Fig. 2*B*) estimates an age of onset of 7.5 wk and an initial rate of 5%/wk lost.

HdhQ111 mice. HdhQ111 mice are another knockin HD model and were also tested in this assay, although we chose to compare HdhQ111 homozygotes to heterozygotes. According to a previous report by the strain's generator, heterozygotes and

homozygotes have few reported differences (28), but if this assay is sensitive it should readily distinguish the two genotypes. Comparing homozygotes to heterozygotes (Fig. 2*A*) also demonstrated progressive GFP loss, beginning at 6 mo of age. As in the CAG140 mice, the decline was significant early on, to 82% of heterozygote levels, but was more variable, ranging between 94% and 67%. By 12 mo of age, homozygote D2GFP had reached 59% of heterozygote levels and variance was minimal in the three mice tested. Power analysis (Table 1) demonstrates a quite robust assay at 12 mo of age, requiring only five mice for detection of a 10% rescue. Compared with heterozygotes, homozygotes begin their D2GFP decline at ~18 wk of age with a 3.1%/wk initial loss rate (Fig. 2*B*).

Table 1. Power analyses for D2GFP levels versus control in HD models

Model	Age	Mean ± SD. GFP	Number to conclude % rescue		
			5%	10%	20%
R6/2	6.5–8 wk	41.2 ± 2.5	6	2	1
	8.5–10 wk	33.1 ± 3.9	11	3	1
	10.5–12 wk	36.6 ± 4.6	17	5	2
R6/1	7 wk	61.3 ± 3.6	28	7	2
	16 wk	34.5 ± 1.8	3	1	1
CAG140	31 wk	61.7 ± 3.1	21	6	2
	36 wk	60.1 ± 3.4	24	6	2
	52 wk	59.4 ± 2.1	9	3	1
HdhQ111	12 mo	58.9 ± 2.9	17	5	2
Q94 AAV	4 wk PI	53.8 ± 4.1	26	7	2

Based on the mean and SDs of the normalized GFP levels (mean ± SD. GFP) for selected cohorts, power analysis was carried out (power = 80%, $P = 0.05$) to determine how many animals would be required to reliably (80% chance) detect a given degree of therapeutic D2GFP rescue at a significance of $P \leq 0.05$. PI, postinfection.

Induction of D2GFP Loss After Delivery of Expanded, but Not Wild-Type, PolyQ HTT Fragments by Adeno-Associated Virus. Having established the utility of the D2GFP reporter system for a series of mouse models, we now asked whether direct introduction of an *mHTT* transgene to the D2GFP MSNs could elicit the same robust GFP loss. We cloned *HTT* exon 1 with either 20 (Q20, nonpathogenic) or 94 (Q94, pathogenic) CAGs into an adeno-associated viral (AAV) vector, which also delivered a red fluorescent protein (RFP) transgene. The AAV constructs were packaged and introduced by stereotactic injection into the striata of 5-wk-old D2GFP mice. After a 4-wk incubation period, striata were harvested and GFP levels were compared between RFP⁺ (infected) and RFP⁻ (uninfected) MSNs (Fig. 3). Neurons expressing Q94 demonstrated a strong and significant GFP loss to 54% of uninfected levels ($P = 0.001$, paired two-tailed Student's *t* test), whereas expression of the Q20 construct did not produce significant GFP loss. This result demonstrates that transcriptional dysregulation can be acutely induced by expression of *mHTT* in adulthood, and that adeno-associated virus represents a rapid means of assessing the impact of *mHTT* on transcript levels.

Demonstration of Therapeutic Impact of an AAV-Delivered shRNA Using the D2GFP FACS Assay. To further determine whether the observed progressive loss of GFP in D2GFP-expressing HD model mice is dependent on mHTT expression and could be alleviated by therapeutic intervention, we produced AAV vectors delivering two genes: RFP, and one of two short hairpin RNAs (shRNAs). shRNAs are short transcripts consisting of sense and antisense sequences of ~21 nt separated by a small loop sequence, and they engage the RNAi machinery in the cell (29),
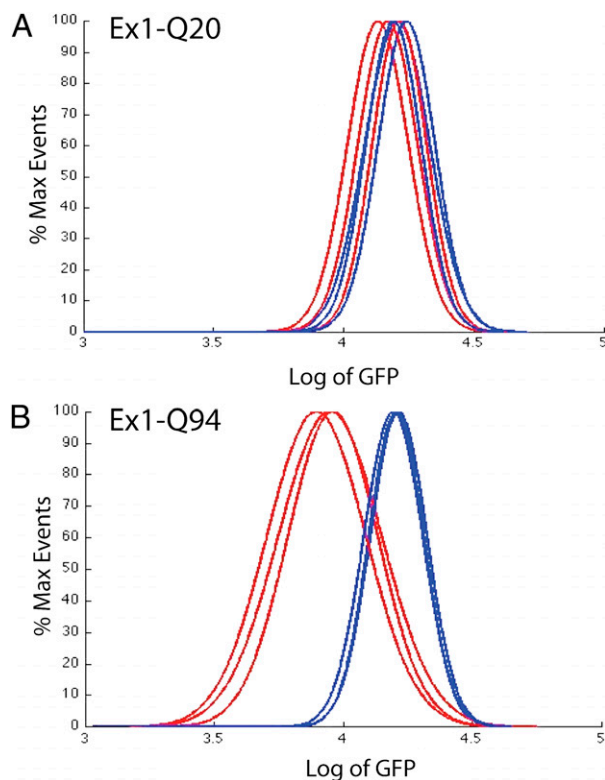
degrading target mRNAs for which perfect complementarity is present. We generated two shRNA sequences, one negative control targeting a transcript absent in the target neurons (*LacZ*, called shLacZ) and one targeting the polyQ tract of HTT (called DhEx1_5). DhEx1_5 can effectively reduce HTT exon 1 protein product (Fig. 4A) by 74% versus shLacZ, as assessed using an HTT exon 1 fusion with luciferase. These AAV genomes were separately packaged into viral particles and delivered to the striatum of 4-wk-old R6/2 mice in the D2GFP background, three mice per vector, and samples were harvested at 8 wk of age (4 wk postinfection).

Note that the expected rescue depends not just on the efficacy of the hairpin but also on the duration of exposure, constrained in this case by the AAV life cycle. AAV-delivered transgenes often take 2–4 wk for peak expression. We have not yet systematically assessed how long it takes an shRNA transgene to reach peak knockdown ability after AAV infection, but if we generously assume it takes 2 wk for mHTT expression to halt and for D2GFP levels to stabilize postinfection, we can use the R6/2 progression curve (Fig. 2B) to predict the maximum rescue. For this experiment, D2;R6/2 mice were injected at 4 wk of age and harvested at 8 wk of age. Halting of D2GFP decline by 2 wk postinfection might cause infected cells' D2GFP levels to resemble those of 6-wk-old mice, estimated to be ~51.9% of control, as opposed to ~39.2% of control in uninfected cells at 8 wk of age. This would represent a 21% rescue (reduction in the amount of D2GFP lost) under ideal conditions, a small dynamic range for most behavioral assays but well above the detection threshold in our D2GFP assay.

After a brief 4-wk incubation, the 8-wk-old mice were killed, striata were harvested, and MSNs were analyzed for GFP content. Comparisons were made within each striatum between the GFP content of RFP⁺ (infected) and RFP⁻ (uninfected) cells. DhEx1_5 partially protected cells from GFP loss upon aging (Fig. 4B). DhEx1_5-expressing cells' GFP levels were reduced to 47% of WT levels, whereas uninfected cells had 39% of WT GFP, representing a rescue of 14 ± 4% in infected cells ($P = 0.01$, paired two-tailed Student's *t* test). This result is consistent with our power analysis (Table 1), which suggests 8-wk-old R6/2 mice require only two mice to detect a 10% rescue in D2GFP loss. Also, this is approximately two-thirds of the maximum rescue (21%) under the aforementioned assumptions of a 2-wk postinfection delay in shRNA expression and arrest of D2GFP loss. The control AAV (shLacZ) had no effect on GFP loss (Fig. 4C).

The shRNA data (Fig. 4) suggest that this AAV system can be used as a rapid, efficient system to assess cell-autonomous effects of the modulation of a target gene on HD transcriptional dysregulation. However, it is worth emphasizing the importance of the disease model's rapidity for the therapeutic window and dynamic range. R6/2 mice have an extremely rapid progression, particularly in our D2GFP dysregulation assay, in which their levels bottom out by only 8 wk of age. If an AAV is going to reach peak expression before the onset of D2GFP loss (4 wk of age), the vector must be introduced to either embryos or pups, which complicates the protocol. On the other hand, if the same experimental paradigm were attempted in CAG140 mice (a strain whose D2GFP decline begins at ~7.5 wk of age), complete rescue of D2GFP dysregulation is plausible, with the tradeoff that this model requires ~7 mo before reaching sufficient power to allow for small cohorts (Table 1).

Discussion

These experiments provide sensitive, quantitative data on the dysregulation of a relevant gene representative of the early stages of polyglutamine toxicity. In addition, the unique protocol presented here permits a number of useful approaches to be taken to support therapeutic development for HD.

Therapeutic Compound Preclinical Testing. For therapeutic modalities that have been identified through cell-based systems or

Fig. 3. A virally delivered mutant *HTT* exon 1 construct induces D2GFP loss. AAV vectors encoding RFP and *HTT* exon 1 (20 or 94 CAGs, termed Q20 and Q94, respectively) were injected into the striata of D2GFP mice at 5 wk of age ($n = 3$ per vector). Four weeks later, striata were processed for FACS and the GFP profiles were compared between RFP⁺ (infected; red trace) and RFP⁻ (uninfected; blue trace) MSNs. Traces for mice receiving Q20 (*A*) and Q94 (*B*) are shown.
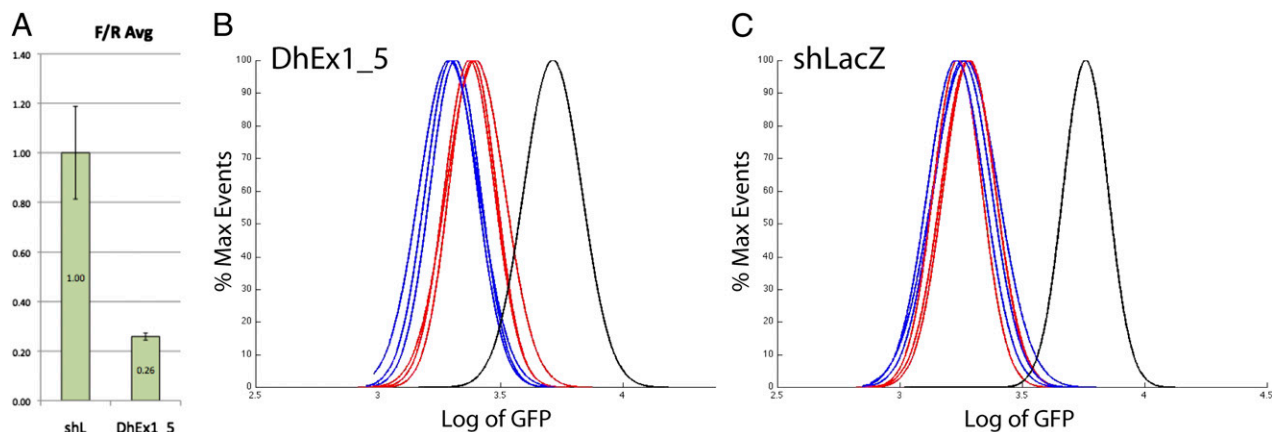
Fig. 4. Knockdown of HTT exon 1 partially prevents GFP loss in D2GFP;R6/2 mice. An shRNA directed against the poly(CAG) tract of HTT exon 1 (DhEx1_5) demonstrated an ~74% reduction of protein expression compared with a nontargeting shRNA (shLacZ) in vitro upon cotransfection with an HTT exon 1-firefly luciferase fusion protein (*A*), normalized to unmodified renilla luciferase (reported as the ratio of firefly/renilla values, or F/R). AAV delivered the shRNA and RFP to 4-wk-old D2GFP;R6/2 striata. Four weeks postinjection, cells carrying DhEx1_5 (*B*; GFP[+] and RFP[+], red trace) showed reduced GFP loss (14 ± 4% rescue, *n* = 3 injected mice, *P* = 0.01) compared with cells without virus (GFP[+] and RFP[−], blue trace). AAV delivering shLacZ (*C*; same color coding as in *B*) failed to demonstrate significant protection (2 ± 8% rescue, *n* = 3 injected mice, *P* > 0.05) from GFP loss. In *B* and *C*, a wild-type littermate (black) was processed in parallel for comparison of GFP decline upon aging in D2GFP;R6/2 mice. *P* values are from a paired Student's *t* test.

chemically based screens, the systems described here provide the opportunity to rapidly and systematically measure efficacy in vivo, at powers facilitating the evaluation of multiple dosages and time points without becoming a practical burden.

Several promising therapies based on modulation of known disease-related pathways have failed at either the preclinical or clinical stages, and this might be the result of correcting one downstream pathway while leaving the many other disease processes uncorrected. A truly promising therapeutic will likely need to target the core pathogenic mechanisms in HD, of which we believe transcriptional dysregulation to be one. It appears early and influences the levels of many genes involved in the highly pleiotropic response to polyglutamine toxicity, suggesting that demonstration of transcriptional normalization could signify a fundamental molecular intervention.

The ability to relatively rapidly and quantitatively measure the impact of therapeutic intervention on a full-length model of disease for HD is of particular importance. From a candidate evaluation perspective, N-terminal fragment models have a more rapid and severe pathology in nearly all known tests compared with full-length models (including CAG140 and HdhQ111), a pattern recapitulated in our assay. The predictability of the D2GFP decline allows one to rapidly pilot potential therapeutics in fragment models and assess efficacy before deciding whether to extend the study to larger cohorts or slower full-length models, which are based on the configuration of the HD expanded repeat in its native environment and are critical for most effectively reflecting the situation encountered in the HD patient. The ability to make a go/no-go decision in a small cohort, within a matter of weeks and with great statistical confidence, may significantly improve the rate of progress in assessing potential HD therapies. To build on this, it will be useful to extend the approach taken here to other full-length mouse models for HD, such as the BACHD lines developed and described by William Yang and his coworkers (30).

Target Validation and Genetic Library Screening. The approach described here also provides the basis for genetic approaches to target validation and genetic screens for novel targets for HD therapy. As we show here, an shRNA against a validated target for HD, the HD gene itself, produces a quantitatively measurable effect in the GFP reporter system. We suggest that the same approach can be taken to validate other targets for HD therapy, and can be rapidly carried out in numerous strains to confirm efficacy across models. We also propose that a group of possible targets can be tested in pools using the AAV-based strategy used here or other

related strategies for introduction of genes into MSNs. We have successfully carried out a preliminary demonstration of this pool-based strategy using high-throughput sequencing as a readout. This modification requires extensive optimization, but provides the potential for forward genetic screens in a minimal number of animals using a relevant metric for cellular health.

Interaction Between Two or More Therapeutic Modalities. For many circumstances, a truly efficacious approach to therapy requires the use of a combination of therapeutic interventions. Such may be the case for HD, as single therapeutic tests rarely produce more than a 20% improvement in R6/2 lifespan, whereas one of the most successful preclinical trials to date, effecting a 32% increase of R6/2 lifespan, was a combination of remacemide and coenzyme Q10 (reviewed in ref. 2). To systematically evaluate the interaction and synergy between two or more therapeutic modalities, particularly in the rapid R6/2 strain for which the therapeutic window is quite narrow, requires a readout that is highly quantitative and reproducible like the one described here. It is our hope that the strategies we describe here will be of particular use in optimizing a therapeutic approach for HD even if several targets or modes of action are necessary to achieve an optimal effect.

Methods

Mice. All procedures were done in accordance with Massachusetts Institute of Technology Committee on Animal Care guidelines. R6/2 mice (~110 CAG repeats) were maintained on a mixed background, either by crossing a transgenic male each generation to B6CBAF1 females or using an ovary-transplanted female bred to B6CBAF1 males. R6/1 (~140 repeats) and CAG140 male mice were bred congenic to C57BL/6, and HdhQ111/111 homozygotes were originally maintained on an outbred CD1 background before homozygosing and interbreeding within a small colony. D2GFP mice were maintained homozygous, congenic to FVB. No differences were observed in progression of the GFP decline phenotype between males and females, and the data were pooled. Animals were weaned at 3 wk of age, housed with one to five mice per cage on a 12-h light/dark cycle, and were fed ad libitum from a wire cage-top hopper.

Dissociation of Neurons into Single-Cell Suspension. The detailed protocol can be found in *SI Methods*. Briefly, mouse striata were dissected, minced with a razor, and incubated with papain and DNase. Neurons were dissociated into a single-cell suspension by trituration with a silanized, polished glass pipette, filtered, and then subjected to flow cytometry. Event-by-event raw GFP quantities were acquired and further processed to assign a GFP level to the population (and therefore the mouse).

Data Processing. Flow cytometry for D2GFP quantitation took place on FACSCalibur or LSRII cytometers (BD). Data were processed with FlowJo software (Tree Star). MATLAB (Mathworks) expectation maximization and Gaussian means regression scripts were used to fit the exported GFP+, DAPI− events to a pair of probability distributions. The mean of the higher GFP distribution was used as the raw GFP value of that sample's MSNs. For mutant mice, this value was normalized to that of one or more simultaneously processed control samples. The script will be provided upon request.

Adeno-Associated Viral Vector Cloning. A vector (pAAV-siRNA) competent for delivery of an shRNA transgene to neurons was acquired from Applied Viromics. For shRNA introduction, one of two sequences was cloned into the siRNA expression region by annealed oligonucleotide ligation. shLacZ forward: 5′-TTTGCGCGATCGTAATCACCCGAGTCTCGAGACTCGGGTGATTACGA-TCGCGTTTTTGG-3′; shLacZ reverse: 5′-CGCGCCAAAAACGCGATCGTAATCAC-CCGAGTCTCGAGACTCGGGTGATTACGATCGCG-3′. DhEx1_5 forward: 5′-TTT-GAGCAGCAGCAGCAGCAACACTCGAGTGTTGCTGCTGCTGCTTTTTTGG-3′; DhEx1_5 reverse: 5′-CGCGCCAAAAAAGCAGCAGCAGCAGCAACACTCGAGT-GTTGCTGCTGCTGCTGCT-3′.

For Q20 and Q94 delivery, the vector was modified through introduction of point mutations to allow for modular insertion of other transgenes downstream of the CAG promoter. Exon 1 of HTT with either 20 or 94 repeats was amplified by PCR and inserted into the region 5′ of RFP using In-Fusion PCR cloning (Clontech). HTT and RFP were separated by a T2a peptide allowing efficient separation. In the Q20 and Q94 vectors, the shRNA region contained the innocuous shLacZ sequence.

shRNA Knockdown Confirmation. 293T cells were seeded onto 24-well dishes and cotransfected with three plasmids: 250 ng of one shRNA construct (shLacZ or DhEx1_5), 10 ng of pGL4.73 (Promega; driving renilla luciferase), and 240 ng of pGL4ex1-Q96 [modified from Promega's pGL4.13, driving expression of a firefly luciferase/HTT exon 1 (Q94) fusion protein]. Media were changed 24 h posttransfection and cells were lysed 48 h posttransfection, and luciferase values were recorded using Promega's Dual Luciferase Kit according to the manufacturer's instructions. Firefly values were normalized to renilla values, and were tested in triplicate.

AAV Production and Purification, and Intracranial Delivery to Mice. Please see *SI Methods* for our detailed protocol on small-scale AAV production and purification, and for the surgical techniques used.

1. The Huntington's Disease Collaborative Research Group (1993) A novel gene containing a trinucleotide repeat that is expanded and unstable on Huntington's disease chromosomes. *Cell* 72:971–983.
2. Crook ZR, Housman DE (2011) Huntington's disease: Can mice lead the way to treatment? *Neuron* 69:423–435.
3. Luthi-Carter R, et al. (2000) Decreased expression of striatal signaling genes in a mouse model of Huntington's disease. *Hum Mol Genet* 9:1259–1271.
4. Kuhn A, et al. (2007) Mutant huntingtin's effects on striatal gene expression in mice recapitulate changes observed in human Huntington's disease brain and do not differ with mutant huntingtin length or wild-type huntingtin dosage. *Hum Mol Genet* 16:1845–1861.
5. Hodges A, et al. (2008) Brain gene expression correlates with changes in behavior in the R6/1 mouse model of Huntington's disease. *Genes Brain Behav* 7:288–299.
6. Strand AD, et al. (2007) Expression profiling of Huntington's disease models suggests that brain-derived neurotrophic factor depletion plays a major role in striatal degeneration. *J Neurosci* 27:11758–11768.
7. Raymond LA, et al. (2011) Pathophysiology of Huntington's disease: Time-dependent alterations in synaptic and receptor function. *Neuroscience* 198:252–273.
8. Andrews TC, et al. (1999) Huntington's disease progression. PET and clinical observations. *Brain* 122:2353–2363.
9. Glass M, Dragunow M, Faull RL (2000) The pattern of neurodegeneration in Huntington's disease: A comparative study of cannabinoid, dopamine, adenosine and GABA(A) receptor alterations in the human basal ganglia in Huntington's disease. *Neuroscience* 97:505–519.
10. Cha JH, et al. (1998) Altered brain neurotransmitter receptors in transgenic mice expressing a portion of an abnormal human Huntington disease gene. *Proc Natl Acad Sci USA* 95:6480–6485.
11. Cha JH, et al. (1999) Altered neurotransmitter receptor expression in transgenic mouse models of Huntington's disease. *Philos Trans R Soc Lond B Biol Sci* 354:981–989.
12. Turmaine M, et al. (2000) Nonapoptotic neurodegeneration in a transgenic mouse model of Huntington's disease. *Proc Natl Acad Sci USA* 97:8093–8097.
13. Hickey MA, et al. (2008) Extensive early motor and non-motor behavioral deficits are followed by striatal neuronal loss in knock-in Huntington's disease mice. *Neuroscience* 157:280–295.
14. Cyr M, Sotnikova TD, Gainetdinov RR, Caron MG (2006) Dopamine enhances motor and neuropathological consequences of polyglutamine expanded huntingtin. *FASEB J* 20:2541–2543.
15. Stack EC, et al. (2007) Neuroprotective effects of synaptic modulation in Huntington's disease R6/2 mice. *J Neurosci* 27:12908–12915.
16. Gong S, et al. (2003) A gene expression atlas of the central nervous system based on bacterial artificial chromosomes. *Nature* 425:917–925.
17. Shuen JA, Chen M, Gloss B, Calakos N (2008) Drd1a-tdTomato BAC transgenic mice for simultaneous visualization of medium spiny neurons in the direct and indirect pathways of the basal ganglia. *J Neurosci* 28:2681–2685.
18. Lobo MK, Karsten SL, Gray M, Geschwind DH, Yang XW (2006) FACS-array profiling of striatal projection neuron subtypes in juvenile and adult mouse brains. *Nat Neurosci* 9:443–452.
19. Gerfen CR, et al. (1990) D1 and D2 dopamine receptor-regulated gene expression of striatonigral and striatopallidal neurons. *Science* 250:1429–1432.
20. Schiffmann SN, Vanderhaeghen JJ (1993) Adenosine A2 receptors regulate the gene expression of striatopallidal and striatonigral neurons. *J Neurosci* 13:1080–1087.
21. Mangiarini L, et al. (1996) Exon 1 of the HD gene with an expanded CAG repeat is sufficient to cause a progressive neurological phenotype in transgenic mice. *Cell* 87:493–506.
22. Li JY, Popovic N, Brundin P (2005) The use of the R6 transgenic mouse models of Huntington's disease in attempts to develop novel therapeutic strategies. *NeuroRx* 2:447–464.
23. Gil JM, Rego AC (2009) The R6 lines of transgenic mice: A model for screening new therapies for Huntington's disease. *Brain Res Brain Res Rev* 59:410–431.
24. Carter RJ, et al. (1999) Characterization of progressive motor deficits in mice transgenic for the human Huntington's disease mutation. *J Neurosci* 19:3248–3257.
25. Wheeler VC, et al. (1999) Length-dependent gametic CAG repeat instability in the Huntington's disease knock-in mouse. *Hum Mol Genet* 8(1):115–122.
26. Menalled LB, Sison JD, Dragatsis I, Zeitlin S, Chesselet M-F (2003) Time course of early motor and neuropathological anomalies in a knock-in mouse model of Huntington's disease with 140 CAG repeats. *J Comp Neurol* 465(1):11–26.
27. Rising AC, et al. (2011) Longitudinal behavioral, cross-sectional transcriptional and histopathological characterization of a knock-in mouse model of Huntington's disease with 140 CAG repeats. *Exp Neurol* 228(2):173–182.
28. Wheeler VC, et al. (2002) Early phenotypes that presage late-onset neurodegenerative disease allow testing of modifiers in Hdh CAG knock-in mice. *Hum Mol Genet* 11:633–640.
29. Xia H, Mao Q, Paulson HL, Davidson BL (2002) siRNA-mediated gene silencing in vitro and in vivo. *Nat Biotechnol* 20:1006–1010.
30. Gray M, et al. (2008) Full-length human mutant huntingtin with a stable polyglutamine repeat can elicit progressive and selective neuropathogenesis in BACHD mice. *J Neurosci* 28:6182–6195.